LASER INTERFEROMETER GRAVITATIONAL WAVE OBSERVATORY
- LIGO -
CALIFORNIA INSTITUTE OF TECHNOLOGY
MASSACHUSETTS INSTITUTE OF TECHNOLOGY

Technical Note **LIGO-T1500123–v1** 2015/05/15

Detector Charactization of a Laser Interferometer Gravitational Wave Detector

Eve Chase
Mentors: Koji Arai and Maximiliano Isi

California Institute of Technology
LIGO Project, MS 18-34
Pasadena, CA 91125
Phone (626) 395-2129
Fax (626) 304-9834
E-mail: info@ligo.caltech.edu

Massachusetts Institute of Technology
LIGO Project, Room NW22-295
Cambridge, MA 02139
Phone (617) 253-4824
Fax (617) 253-7014
E-mail: info@ligo.mit.edu

LIGO Hanford Observatory
Route 10, Mile Marker 2
Richland, WA 99352
Phone (509) 372-8106
Fax (509) 372-8137
E-mail: info@ligo.caltech.edu

LIGO Livingston Observatory
19100 LIGO Lane
Livingston, LA 70754
Phone (225) 686-3100
Fax (225) 686-7189
E-mail: info@ligo.caltech.edu

http://www.ligo.caltech.edu/

1 Introduction

Einstein's General Theory of Relativity propelled a scientific hunt for the detection of gravitational waves. Einstein's equations establish the dynamics of space-time, a four-dimensional mathematical model combining the dimensions of space and time. General relativity predicts the existence of gravitational waves, propagating ripples in space-time. Gravitational waves are transverse waves, predicted to travel at the speed of light, produced by the change in quadrupole moment of mass distribution [1]. Nearly a century after their inception, gravitational waves have yet to be directly detected.

A worldwide network of ground-based interferometers has been constructed to provide the first direct detection of gravitational waves. The Laser Interferometer Gravitational-Wave Observatory (LIGO), consisting of detectors in Livingston, Louisiana and Hanford, Washington, recently underwent years of upgrades to provide greater sensitivity and increase the likelihood of detecting gravitational waves. A gravitational wave detector is a massive Michelson interferometer, with arm lengths of up to 4km (Figure 1) [3]. Laser light is split and sent down two orthogonal arms of equal length; the light is reflected at the end of the arms and then recombined. When a gravitational wave passes through an interferometer, a slight change in arm length will occur, resulting in a phase difference in laser light split down each arm. Gravitational wave signals are extracted from this resultant phase difference.

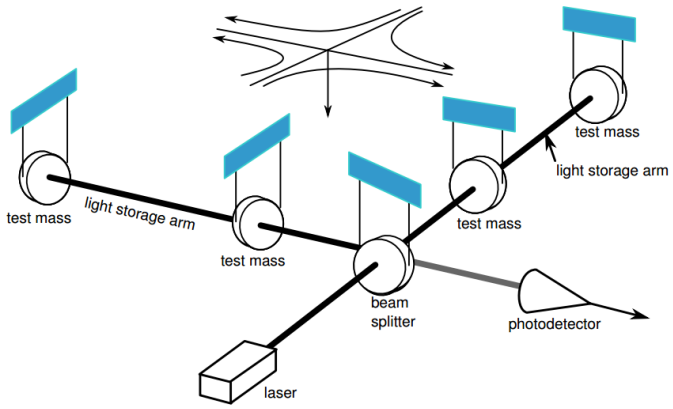

Figure 1: Basic interferometer design (LIGO [2])

Detecting a gravitational wave is difficult and requires impeccably sensitive instrumentation and detection abilities, in an attempt to detect length variations of only 10^{-18} m, smaller than a proton [3]. Everything in the interferometer system is moving or fluctuating, such as the mirror position, laser frequency, laser intensity, arm resonant condition, and many more factors resulting in a substantial number of noise sources. Gravitational wave detection is a battle against noise, and detector characterization spearheads this battle. Through detector characterization, we analyze interferometer output and noise sources for certain periods of time to characterize the nature of noise, in hopes of eliminating it from the data supply. Gravitational waves cannot be detected with LIGO without strong detector characterization techniques.

As Advanced LIGO becomes operational in late 2015 [4], the implementation of advanced

detector characterization techniques is imperative to utilize the increased sensitivity for direct detection of gravitational waves. I am excited to devote my summer to LIGO detector characterization while it serves a vital role in the effort to detect gravitational waves. I hope to use my previous LIGO work in conjunction with my programming experience to provide meaningful contributions to a summer research project.

My summer project will consist of two main parts, outlined in this paper. As described in Section 2, I will update the LIGO summary pages which accomplish detector monitoring tasks. Subsequently, I will characterize non-Gaussian noise through various statistical methods, as described in Section 3. I provide a timeline for my summer work in Section 5.

2 Summary Pages

In addition to the two large LIGO detectors in Washington and Louisiana, Caltech houses a prototype detector [5]. The prototype detector, with 40m long interferometer arms, has a similar configuration to the larger detectors but is open to modification and testing of new design implementations (Figure 2). The 40m prototype detector is the perfect playground for detector characterization experimentation. We are able to devote much more time to in-depth investigations without hesitating to disrupt data collection. By disrupting data collection at the 40m detector instead of the LIGO sites, we are able to provide novel improvements to all LIGO detectors without interfering with data collection at the sites. The prototype consists of several subsystems which monitor the functionality of the detector, enumerated in Table 1 [6, 7, 8]. By frequently collecting data from the subsystems, we provide a means of monitoring the detector.

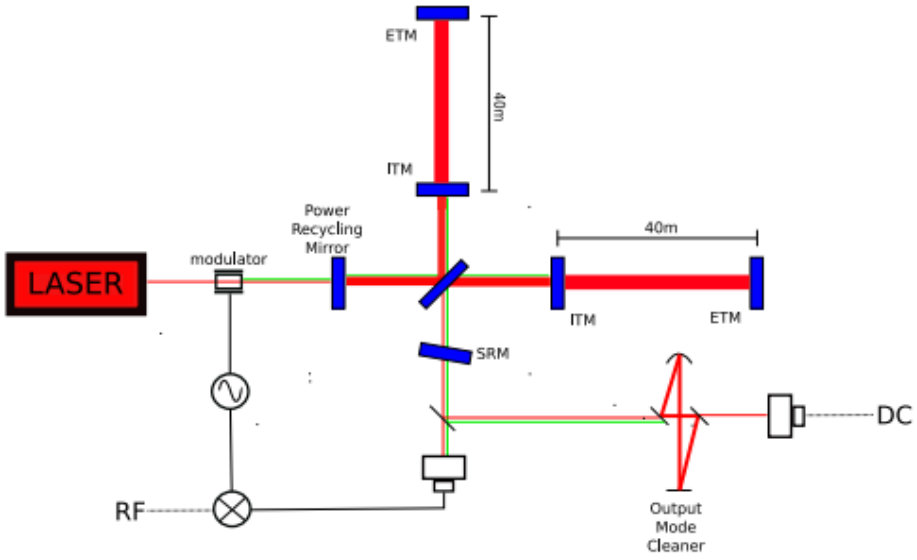

Figure 2: Schematic representation of the 40m prototype detector. A length of 40m separates the input mirror (ITM) and end mirror (ETM) [6] (Ward et al. [5]).

LIGO summary pages provide an accessible method to monitor the detectors in real time

Table 1: 40m Detector Subsystems

Name	Subsystem Details
Length Sensing and Control (LSC)	Mirror position control and gravitational wave signal channel.
Angular Sensing and Control (ASC)	Mirror angular control.
Pre-Stabilized Laser (PSL)	Optical cavities for laser stabilization in frequency and spacial distribution.
Input and Output Optics (IOO)	Similar to PSL.
Suspensions (SUS)	Sensors for mirror positions and angles. Optical lever system which provides additional angular sensing signals.
Physical Environmental Sensors (PEM)	Seismic and acoustic noise.
Vacuum System (VAC)	Vacuum status monitoring.

on-line [9]. Summary pages include dozens of plots monitoring detector status from seismic activity, to glitches, and to lock status. Summary pages include ASD spectra displaying gravitational wave amplitude spectral density over frequency [10]. Summary pages also provide time-frequency event plots represent signal-to-noise ratio (SNR) for several event triggers [10]. A screenshot of summary pages is shown in Figure 3. While the Hanford and Livingston detectors utilize summary pages, the 40m detector has few features implemented on the summary pages. The 40m summary pages are far behind the quality of the Livingston and Hanford summary pages and lack much of the information represented in the latter two [9, 11, 12]. We hope to provide a legible, informative summary page interface to improve upon the currently existing channel visualization for the 40m prototype.

Implementation of summary pages for the 40m prototype requires careful configuration of many channels from many subsystems of the prototype. We analyze each channel for a set period of time to determine the nature of each signal. While checking the behavior of signals, we may reveal problems with the functionality of specific subsystem of the detector, contributing to detector improvement.

Summary pages are produced using the GWsumm toolbox, which is based on the GWpy Python package which provides tools to load, assess, and plot LIGO data. GWsumm scripts can provide plots for data channels and associated HTML to post the plots on the summary page website. A significant portion of my summer will be spent characterizing data channels for the 40m detector and implementing them into the summary page system.

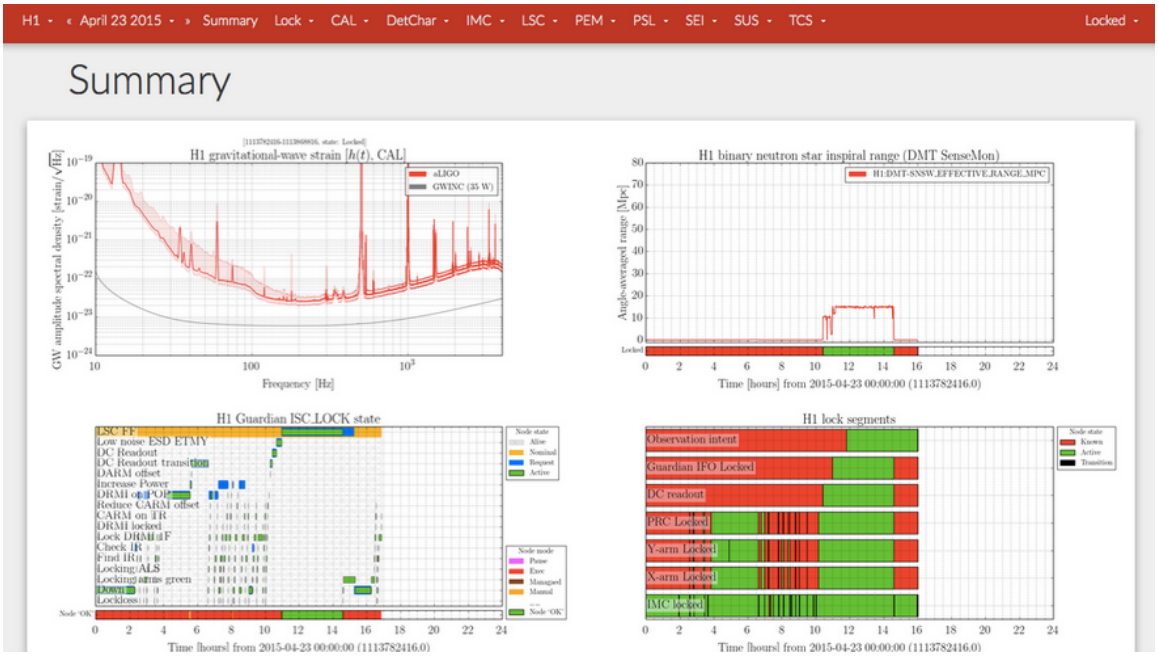

Figure 3: Screenshot of a summary page monitoring the Hanford detector [12].

3 Non-Gaussianity Tests of Noise Sources

While not working on implementation of summary pages, I will work on noise characterization. We explore how various noise sources appear in the interferometer channels and provide additional methods to characterize noise with the predefined goal of eliminating as many noise sources as possible from the detector.

Gravitational wave detectors are constantly inundated with noise. Noise comes in numerous forms, such as white noise, sinusoidal, stochastic, Gaussian, and more. Sources of white noise include quantum noise and electronic noise with broad frequency bands. Sinusoidal noise sources such as narrow band sources and noise from power lines at 60Hz are also present, in addition to narrow band stochastic noise sources such as thermal noise in mirror suspension wires. Other sources of noise include seismic noise. We can categorize noise as Gaussian or non-Gaussian, dependent on the statistical nature of the noise. Typically, thermal and quantum noise exhibit Gaussian behavior. It is difficult to distinguish between gravitational wave events and non-Gaussian noise, thus requiring the characterization of non-Gaussian noise to reveal true event signals [13]. By characterizing noise as Gaussian or non-Gaussian, we can better recognize noise patterns and understand the nature of noise, leading to the further elimination of many noise sources.

Rayleigh statistics provide one means to determine the Gaussianity of a noise distribution [7, 14]. The Rayleigh statistic (R) provides a metric for the Gaussianity of noise through a calculation of the standard deviation and mean of a power spectrum in various frequency bins:

$$S(f) = \frac{1}{N}\sum_{i=1}^{N} |X_i(f)|^2 \,. \tag{1}$$

$$R(f) = \frac{\sigma[|X_i(f)|^2]}{\mu[|X_i(f)|^2]}, \tag{2}$$

where σ and μ are defined in Appendix A and X is a Rayleigh random variable. The set of all X's composes the Rayleigh distribution. The value of R provides a numerical measure of the Gaussianity of a signal, with an $R = 1$ representing Gaussian noise, an $R < 1$ representing coherent variation in the data, and an $R > 1$ indicating that glitchy data is present [7, 14]. The RayleighMonitor algorithm can be used to plot spectrograms (μ) and Rayleighgrams (R) for a visual representation of detector characterization [14, 15]. By inputting data from an arbitrary set of channels, we receive output of time-frequency plots for both power spectrum and Rayleigh Statistics [15].

Power spectral density (PSD) provides another means to characterize noise distributions. A PSD is a measure of power in several frequency bans, averaged over time. We create a PSD by first calculating a spectrogram, which is a time-domain change in a noise power spectrum calculated from the output data of the interferometer using a fast Fourier transform (see Appendix A). A spectrogram provides noise power fluctuations at each frequency bin which are then added to provide a PSD [13]. We follow a similar method to that outlined in Ando et al. [13] in which the average power (P_1) and second-order moment of the power (P_2) are calculated at once for frequencies between 400 Hz and 1.3kHz. Two evaluation parameters,

$$c_1 = \frac{P_1}{P_0} - 1 \tag{3}$$

and

$$c_2 = \frac{1}{2}\left(\frac{P_2}{P_1^2} - 2\right) \tag{4}$$

are calculated, in which P_0 represents an average power over a longer period of time. It is assumed that c_2 becomes constant if the signal power is much larger than the background noise level [13]. Statistics based on the ratio of c_1-to-c_2 provides a useful measure in detector diagnosis through PSD. Unlike the methods described in Ando et al. [13], we will calculate a spectrogram providing power information at a each frequency bin, as opposed to a lump sum in a set range of frequencies. This allows us to evaluate statistical parameters such as c_1 and c_2 as a function of frequency, possibly illuminating differences in noise sources at different frequencies.

We will calculate PSDs of interferometer signals for a given short period of time, providing many useful applications in detector characterization. For example, PSD calculation will allow us to monitor the violin, roll, and bounce modes of the steel wires used to suspend the interferometer's mirrors. Each mirror has six rigid body degrees of freedom: longitudinal, side, vertical, pitch, yaw, and roll. The resonances of each of these six modes has low dissipation, corresponding to a long ringdown mode, or high quality factor (Q) for the modes. Feedback damping is used to lower the Q's for some modes, but the violin, roll, and vertical (or bounce) modes have no such damping control and occasionally become excited

by seismic motion or cross-coupling between modes. Characterization of noise from these three modes can be achieved through the calculation of a PSD.

We will calculate both Rayleigh statistics and a PSD for interferometer signals at each predetermined frequency bin and plot PSD and R in the same figure. We are interested in determining the relationship between Rayleigh statistics and PSD and also hope to determine how Gaussianity depends on the size of the time series segment used for calculation. By characterizing the Gaussianity of noise, we hope to provide a better understanding of noise sources at the interferometer and eliminate these noise sources in data requisition.

4 Conclusion

As Advanced LIGO begins to collect data, detector characterization takes a vital role in the effort to locate gravitational wave signals in this data. It is imperative to distinguish between gravitational wave events and non-Gaussian noise signals in order to detect gravitational waves, specifically bursts [13]. The implementation of summary pages for the 40m prototype detector benefits the entire LIGO community by providing real-time access to detector monitoring tools for the interferometer and providing improvements to the summary pages, which may be incorporated into summary pages for the main detectors. In the upcoming race to directly detect gravitational waves with a ground-based interferometer, detector characterization is vital in the understanding and elimination of noise.

5 Timeline

Upon arrival at Caltech on June 16, I will begin preliminary work to understand the coding mechanisms behind the summary pages and channel characterization for the 40m detector. After a few weeks of acclimating myself with the available code, I will begin work on the characterization of non-Gaussian noise sources while simultaneously implementing detector monitoring tools for the 40m detector summary pages. By August 21, I hope to produce a final paper describing my progress over the summer.

References

[1] Flanagan, E. & S. Hughes. *The basics of gravitational wave theory.* New J.Phys. 7, 204 (2005).

[2] http://www.ligo.caltech.edu/LIGO_web/PR/scripts/draw_lg.html

[3] Abbott, BP et al. *LIGO: the Laser Interferometer Gravitational-Wave Observatory.* Rep. Prog. Phys. 72, 076901 (2009).

[4] https://www.advancedligo.mit.edu/

[5] Ward, RL et al. *DC Readout Experiment at the Caltech 40m Prototype Interferometer.* Class. Quantum Grav. 25, 114030 (2008).

[6] Izumi, K. et al. *Multicolor cavity metrology*. J. Opt. Soc. Am. 29, 10, 2092 (2012).

[7] Davison, E. *Detector Characterization Tools for Interferometer Commissioners*. LIGO SURF 2012.

[8] Abbott, B. et al. *LIGO Caltech 40-Meter Prototype Procedures Manual*. 2003.

[9] http://www.ligo.caltech.edu/~misi/summary/

[10] Macleod. *How to read the (LIGO) summary pages*.

[11] https://ldas-jobs.ligo-la.caltech.edu/~detchar/summary/

[12] https://ldas-jobs.ligo-wa.caltech.edu/~detchar/summary/

[13] Ando, M. et al. *Methods to characterize non-Gaussian noise in TAMA*. Class. Quantum Grav. 20, S697 (2003).

[14] Sutton, P. & P. Saulson. *RayleighMonitor Overview*. LIGO-G040422-00-Z.

[15] Finn, L., Gonzalez, G. & P. Sutton. *RayleighMonitor: A Time-Frequency Gaussianity Monitor for the DMT*. LIGO-G020133-00-Z (2002).

[16] http://hyperphysics.phy-astr.gsu.edu/hbase/math/fft.html

Appendix A Relevant Statistical Concepts

A.1 Arithmetic Mean

The arithmetic mean represents an unweighted average of a set of n values.

$$\mu = \overline{x} = \frac{1}{n}\sum_{i=1}^{n} x_i \tag{5}$$

A.2 Variance

Variance, σ^2, measures the spread of a set of numbers.

$$\sigma^2 = \frac{1}{n}\sum_{i=1}^{n}(x_i - \mu)^2 \tag{6}$$

A.3 Standard Deviation

Standard deviation is the square root of variance. It represents the amount of variation in a set of n values.

$$\sigma = \sqrt{\frac{1}{n}\sum_{i=1}^{n}(x_i - \mu)^2} \tag{7}$$

A.4 Skewness

Skewness quantifies the asymmetry of a distribution. If the left side is more pronounced than the right side, then the data set is said to have negative skewness. If the distribution is symmetric, skewness is zero. Equations for skewness vary, and one such equation is provided below.

$$Skewness = \frac{\frac{1}{n}\sum_{i=1}^{n}(x_i - \mu)^3}{\sigma^3} \tag{8}$$

A.5 Kurtosis

In addition to skewness, kurtosis provides another descriptor for the shape of a distribution. Kurtosis is represented in many ways, of which one such equation is provided, and can be thought of as "peakedness" of a distribution.

$$Kurtosis = \frac{\frac{1}{n}\sum_{i=1}^{n}(x_i - \mu)^4}{\sigma^4} \tag{9}$$

A.6 RMS

The root mean square (RMS) can be calculated to represent a series of data points varying with time. The RMS for a set of n discrete values is:

$$x_{rms} = \sqrt{\frac{1}{n}(x_1^2 + x_2^2 + \cdots + x_n^2)}, \tag{10}$$

while the RMS for a continuous time-dependent function from the time interval T_1 to T_2 is

$$f_{rms} = \sqrt{\frac{1}{T_2 - T_1}\int_{T_1}^{T_2}[f(t)]^2 dt}. \tag{11}$$

A.7 Fourier Transform

The Fourier transform provides a continuous Fourier series from $-\infty$ to ∞ for a given function. The Fourier transform of $f(t)$ is,

$$g(\omega) = \frac{1}{2\pi} \int_{-\infty}^{\infty} f(t) e^{-i\omega t} dt, \tag{12}$$

and the inverse Fourier transform is,

$$f(t) = \int_{-\infty}^{\infty} g(\omega) e^{i\omega t} d\omega. \tag{13}$$

A.8 Fast Fourier Transform

The fast Fourier transform (FFT) provides a model for transforming a function of time into a function of frequency. Rather than describing the mathematical formalism of a FFT, I will express its overall function pictorially in Figure 4.

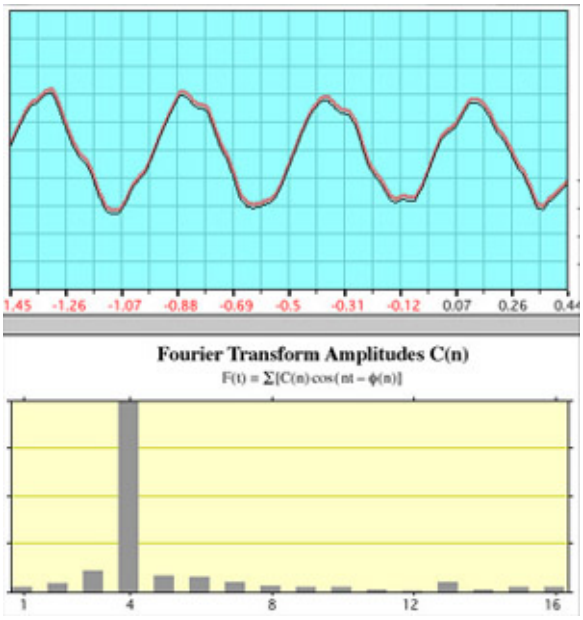

Figure 4: The bottom plot displays the FFT of the above plot. The FFT shows that most of the power is at frequency 4, reflecting the fact that four periods were chosen for the calculation of the FFT [16].

A.9 Parseval's Theorem

Parseval's Theorem illuminates the relationship between the average of the square of a function $f(t)$ and the Fourier coefficients. Assume a function f(t) is represented by the following Fourier series:

$$f(t) = \sum_{-\infty}^{\infty} c_n e^{in\pi t/l}, \tag{14}$$

where c_n is

$$c_n = \frac{1}{2l}\int_{-l}^{l} f(t)e^{-in\pi t/l}dt. \tag{15}$$

Parseval's Theorem then claims the following:

$$\text{The average of } |f(t)|^2 \text{ over a period} = \sum_{-\infty}^{\infty} |c_n|^2 . \tag{16}$$

Parseval's Theorem can easily be related to the RMS by the inclusion of a square root.